International Journal of Pavement Research and Technology (2024) 17:151–168
https://doi.org/10.1007/s42947-022-00225-3

社團法人中華鋪面工程學會
Chinese Society of Pavement Engineering

ORIGINAL RESEARCH PAPER

Roller Compacted Concrete with Oil Shale Ash as a Replacement of Cement: Mechanical and Durability Behavior

Ahmed M. Ashteyat[1] · Yousef S. Al Rjoub[2] · Ala'Taleb Obaidat[3] · Mehmet Kirgiz[4] · Mu'atsem Abdel-Jaber[5,1] · Amani Smadi[2]

Received: 5 October 2021 / Revised: 1 August 2022 / Accepted: 3 August 2022 / Published online: 13 September 2022

Abstract

Oil shale is considered an important source of energy production; however, the burning of oil shale produces deposits that are difficult to be disposed of, which results in serious damage to the environment around us. Since Jordan contains abundant amounts of oil shale, the need to find alternative solutions for exploiting this deposit has become essential. This study aims to investigate the possibility of utilizing oil shale ash (OSA) in the cement industry as a partial replacement for cement in the production of roller-compacted concrete (RCC). Cement was replaced by OSA with replacement levels of 0%, 10%, 20%, 30%, and 40%. Standard cylinders, cubes, and prisms were used to examine the physical properties (density and porosity), mechanical properties (compressive strength, splitting tensile strength, flexural strength, and modulus of elasticity) and durability (Ultrasonic Pulse Velocity (UPV), and compressive strength after cycles of freezing–thawing) of RCC mixes. The results indicated that using OSA at different replacement levels has significantly affected the mechanical properties of RCC mixes as they decreased with the increase of OSA content in the mix but at different rates. The reduction in compressive strength, splitting strength, flexural strength, and modulus of elasticity of RCC was 18–42%, 27–37%, 3–61%, and 3–61%, respectively. However, RCC with OSA reached the required compressive stress for roller compacted concrete that could be used for public traffic or dams according to American Concrete Institute (ACI) requirements. The durability behavior was satisfactory in RCC with different OSA replacement levels compared to control RCC. Based on the experimental results, it is possible to use OSA in producing RCC for up to 30% as a main base coarse.

Keywords Oil shale ash · Supplementary cementitious material · Sustainable roller-compacted concrete · Microstructure · Physical properties · Mechanical properties · Durability · Elasticity

1 Introduction

The most significant mix constituent of concrete is the cement that emits not only carbon dioxide (CO_2) but also nitrogen oxides (NO_x) and methane (CH_4). Cement production is an extensive energy-consuming process and is estimated to be responsible for about 7% of total global carbon dioxide (CO_2) emissions each year [1, 2]. In near future, the manufacture of Portland cement will remain very concerning to population growth in the world. In 1880, cement manufacturing was 2 million tons, and it increased to 5 billion tons in 2019 [3]. To minimize the harmful effects of

✉ Ahmed M. Ashteyat
a.ashteyat@ju.edu.jo

Yousef S. Al Rjoub
ysalrjoub@just.edu.jo

Ala' Taleb Obaidat
atobaidat@gmail.com

Mehmet Kirgiz
nakres42@yahoo.com

Mu'atsem Abdel-Jaber
m.abduljaber@ju.edu.jo; M.abdeljaber@amman.edu.jo

[1] Department of Civil Engineering, The University of Jordan, Amman 11942, Jordan

[2] Department of Civil Engineering, Jordan University of Science and Technology, Irbid, Jordan

[3] Civil Engineering Department, Philadelphia University, Amman, Jordan

[4] Istanbul Sabahattin Zaim University, Istanbul, Turkey

[5] Department of Civil Engineering, University of Jordan on Sabbatical leave at Al-Ahliyya Amman University, Amman 19328, Jordan

cement consumption, cement is partially replaced with supplementary cementitious materials (SCMs) such as oil shale ash, marble powder, rice husk ash, pulverized fuel ash, calcined clay, ground granulated blast furnace slag, and limestone powder, etc., in the cement-based materials mixture.

The demand for green materials and cost reduction in the construction industry has led to a current model for reuse, recycling, and upcycling of various wastes from various goods manufacturing in the cement-based eco-friendly material system. One of the wastes essentially used is oil shale ash (OSA), which contains very valuable chemical oxides. OSA is generated by the oil industry, more than two hundred fifty billion tons in the world [4]. The burning of oil shale for manufacturing the fuel-based energy is the main source of the OSA. The environmental problems related to the production of OSA and the high cost of its disposal have attracted most researchers to examine its potential to be used in the cement and concrete industry or soil [5–26]. Table 1 summarizes several research on using oil shale ash in soil and concrete. Results showed that the strength development rate of OSA-based concrete depends on the combustion temperature which changes the properties of produced ash [8–10]. Replacement of cement by larger than 10% has a negative effect on the concrete mechanical properties [11, 15]. Also, increasing the water binder ratio will decrease the compressive strength of OSA concrete [7, 11, 13].

RCC was identified by ACI as concrete compacted by a roller that squashes the concrete in its fresh stance to form the RCC [27]. The RCC has a similar constituent of traditional concrete mixing, with a broad range of materials and a low water-to-cement ratio (w/c). Its w/c is between 0.2 and 0.4, and the aggregate gradation has different requirements compared to normal concrete, and it needs the SCMs as additives. RCC consistency requirement is different from traditional concrete in use. Mixing should be dry enough to be compacted by a roller vibrator, and the mixing water should be sufficient to wet the aggregate stack and to start the hydration process of its binder during the mixing and compaction [27]. The RCC provides the strength and performance required as being in the conventional concrete, as well as reducing the oil-based asphalt use [28–30].

Table 1 Summary of the literature on using OSA

Title	Author	Study area
Producing geopolymer composites using oil shale ash	5	Geopolymer concrete
Effect of burnt oil shale on ASR expansions: a petrographic study of concretes based on reactive aggregates	7	Concrete
Oil shale ash based backfilling concrete—Strength development, mineral transformations and leachability	8	Concrete
Treated oil shale ashes as a substitute for natural aggregates, sand, and cement in concrete	17	Concrete
Composıtıon and propertıes of oıl shale ash concrete	10	Concrete
Production of self-compacting concrete using Jordanian oil shale ash	15	Self-compacting concrete
Evaluation of New Applications of oil shale ashes in building materials	12	Clay brick
Cement-based materials with oil shale fly ash additives	13	Concrete
Characterızatıon and utılızatıon of oıl shale ash mıxed wıth granıtıc and marble wastes to produce lıghtweıght brıcks	16	Bricks
Production of ceramics from waste glass and Jordanian oil shale ash	25	Ceramic
Durability behavior of Portland burnt oil shale cement concrete	11	concrete
The effect of partial replacement of cement by virgin Oil Shale Powder and/or Oil Shale Ash on properties of cement mortar (comparative study)	14	mortar
Leaching behaviour of Estonian oil shale ash-based construction mortars	18	mortar
The use of oil shale ash in Portland cement concrete	19	Mortar and concrete
Potential uses of Jordanian spent oil shale ash as a cementive material	20	Mortar
The Use of Jordanian Oil Shale Ash as a Soil Stabilizing Agent	21	Soil stabilization
The Use of Oil Shale Fly Ash to Improve the Properties of Irbid Soil	6	Soil stabilization
Influence of waste products from electricity and cement industries on the thermal behavior of Estonian clay from Kunda deposit	22	Soil stabilization
Effect of grinded oil shale inclusion on some properties of concrete mixtures	23	concrete
Behavior of concrete made using oil-shale ash and cement mixtures	24	concrete
Durability performance and engineering properties of shale and volcanic ashes concretes	9	concrete
Roller compacted concrete with oil shale ash as a replacement of cement: mechanical and durability behavior	Current study	Roller compacted concrete (RCC)

The RCC used for dams usually contains a higher volume of pulverized fuel ash and/or other types of supplementary cementitious materials. The maximum quantity of the pulverized fuel ash used in the RCC for pavement mixing is usually 20% of the total binder mass. Regularly, using the pulverized fuel ash in the RCC mixing increases the fine material and leads to higher yielding homogeneous paste and greater consistency [31]. Different by-products such as silica fume, marble powder, limestone dust, brick powder, graphite nanoparticle, ground granulated blast furnace slag, and rice husk ash could be enumerated among other SCMs used extensively in the RCC mixing, and they could improve the strength, density, and the frost resistance of RCC [32–57]. Debbarma et al. [32] used reclaimed asphalt pavement (RAP) in the production of roller compacted concrete pavement (RCCP) mixes. The results showed that the incorporation of any fraction of RAP could reduce the compressive, flexural, and split tensile strength of RCCP mixes significantly at all curing ages. Also, none of the RAP mixes could achieve the recommended compressive strength criterion of 27.6 MPa. Fine RAP mixes were found to exhibit better strength properties than coarse RAP and combined RAP mixes. Another study on using RAP and recycled aggregate concrete (RCA) in producing RCC was conducted by [33]. The results showed that replacing the NA aggregates with RCA and RAP in RCC mixtures has decreased the mechanical properties such as compressive, splitting strength flexural strength and modulus of elasticity. Even though the RCC reached the required compressive strength which would be used for public traffic or dams.

Rahmani et al. [36] evaluated the mechanical properties of RCCP and compared them with those of normal concrete using existing international codes and predictive models. In the experimental study, 11 mixtures of RCCP with various water-to-cement (W/C) ratios (0.3–0.55) and various cement content values (240–340 kg/m^3 were cast. The test results showed that decreasing the W/C ratios from 0.55 to 0.3 increased the Vebe time up to two times while increasing the cement content from 12% to 17% decreased the Vebe time by 34%. In addition, the results showed that decreasing the W/C ratios and increasing the cement content cause the physical and mechanical properties of RCCP to improve. The compressive strength, of RCCP, was almost doubled by decreasing the W/C ratio from 0.55 to 0.3. The dry unit weight, ultrasonic pulse velocity, and dynamic modulus of elasticity of RCCP increase when decreasing the W/C ratio as well as increasing the cement content of RCCP.

Bayqra et al. [40] investigated the physical and mechanical properties of high-volume fly ash roller compacted concrete pavement. In the designed mixes 60% (by weight of cement) of either cement or aggregate was replaced with fly ash (FA). In the laboratory, the specimens with and without 1 cm interlayer mortar were prepared in two layers and compacted by a vibrating hammer. For the field study, platforms 100 cm long, 80 cm wide, and around 40 cm (compacted) depth were produced from each mixture. Results showed that placement of the RCC in two layers, even without any delay in placement and compaction of the top layer, caused interlayer cold joint and subsequent reduction in the strength. Also, laboratory specimens with and without interlayer bedding mortar showed higher strength than the similar field (core) specimens.

Rooholamini et al. [41] studied the effect of partial and full replacement of natural aggregate with the Electric Arc Furnace (EAF) steel slag on the mechanical and fracture properties of Roller Compacted Concrete (RCC). In the study RCC specimens incorporating fine or coarse EAF slag aggregate were prepared and different test methods of compressive, splitting tensile, pull-off adhesion and flexural strength were employed to evaluate them. The results showed that for fine aggregate replacement, the mechanical properties decreased by an increase in the amount of EAF steel slag, which has a high specific surface area. Besides, incorporating the coarse EAF steel slag increased aggregate interlock mostly due to its high angularity and roughness causing to promoting mechanical and fracture properties.

Rahmani et al. [42] studied the effect of cement content (cement to aggregate ratio) on the fracture parameters and ductility of Roller compacted concrete pavement (RCCP). Several cement-to-aggregate ratios (from 12% to 17%) were used in the experimental program. Boundary effect method (BEM), size effect method (SEM), and work of fracture method (WFM) were employed to assess the parameters of fracture. The results indicate that in the RCCP mixes, with raising the cement aggregate ratio the total fracture energy (GF) and initial fracture energy (Gf) increased. The characteristic length (Lch) indicates the brittleness of concrete in WFM, slightly decreased (by around 11%) as a result of raising the cement content (raising cement to aggregate ratio 12% to 17%), which suggests that the RCCP mixes became more brittle as their cement content increased.

Aghayan et al. [46] studied the mechanical properties, and durability of roller-compacted concrete pavement containing recycled waste materials. In the study, ceramic waste aggregates were used at 10%, 15%, 20%, and 25%, by the weight of coarse aggregates. While coal waste powder was used in the mixture at the replacement levels of 4% and 8% by the weight of cement. The results showed that the use of ceramic waste as aggregates increased the vibrating compaction time of fresh mixtures while decreasing their density. Also, coal waste powder reduced the vibrating compaction time of RCCP mixtures. The results showed that 90-d compressive, splitting tensile and flexural strengths were increased by 14%, 39%, and 20%, respectively, after replacing 15% of natural

aggregates with ceramic waste. Also, using ceramic waste aggregate increased the durability of concrete after 90-d curing time.

In light of the above-mentioned previous studies, and as shown in Table 1, it is clear the need to study the effect of using OSA as a replacement for cement in producing RCC due to the lack of research conducted on this topic. Therefore, this research will evaluate the efficiency of using OSA as a substitution material for cement in roller compacted concrete composite mixing. Each 12 million tons of coarse aggregates consumed in asphalt application every year generates 2.4 million tons of CO_2 emission, and if the RCC were used in all roads in the world, there would be a saving in the cost of oil-based asphalt material alone of $15 billion, and the problem of disposal of such by-products as the OSA and the plastic generated from oil manufacturing would cease to exist.

2 Experimental Program

2.1 Materials

2.1.1 Cement

Type I Portland cement was used in preparing the RCC for experiments carried out in the study. The chemical properties of ASTM type I cement are shown in Table 2.

2.1.2 Aggregates

The aggregates used for the production of RCC mixes are a combination of coarse aggregates, fine aggregates, and silica sand (55% coarse aggregate and 40% fine aggregate, and 5% silica sand). The specific gravity and water absorption were calculated according to ASTM C128 [58]. For coarse aggregates, the specific gravity and water absorption were 2.62 and 1.5%, respectively, while for fine aggregates, the results were 2.58 and 4.5%, respectively (Fig. 1).

Table 2 Chemical properties of ASTM type I cement

Types of cement	Chemical properties (%)										
	CaO	SiO_2	AL_2O_3	Fe_2O_3	MgO	SO_3	Na_2O	K_2O	Alkali	TiO_2	Loss in ignition
ASTM Type I	64	20	4.69	3.78	2.46	2.27	0.02	0.4	0.265	–	0.78

Fig. 1 The oil shale ash output, and its main sources [26]

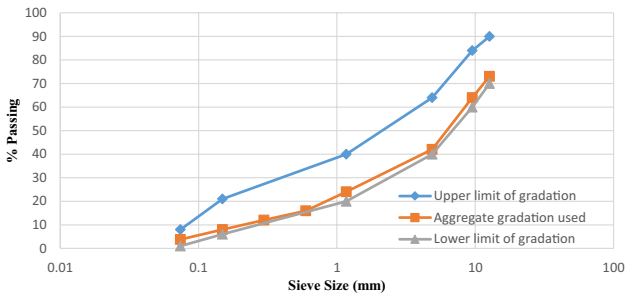

Fig. 2 Sieve analysis of aggregate

Fig. 3 The OSA obtained after crushing, burning, and grinding

Table 3 Sieve analysis of OSA

Sieve size (μ)	20	45	63	90	15
% Retained	55–60	18–22	9–12	2.5–4.5	0–0.9

Sieve analysis and fineness modulus were conducted for the aggregates according to ASTM C136 standard [59], however, the fineness modulus of the fine aggregates was 2.7. Figure 2 presents the gradation of aggregates used in the RCC mixes along with the upper and lower limits.

2.1.3 Oil Shale Ash (OSA)

The oil shale rocks were obtained from the southern part of Jordan. The rocks were crushed and then burned at a temperature of 650 °C for 6 h. After that, the oil shale rock chunks were ground to the required size and used to substitute the cement in RCC mixes, as seen in Fig. 3. The OSA particles have Blaine fineness of 550 kg/m^2 and specific gravity of 2.69. Table 3 shows the particle size distribution of OSA.

It can be seen from Fig. 4 that the OSA has various amorphous and geometrical shapes such as angular, tetragonal, pentagonal, and hexagonal with a rough and porous surface as shown in the micrograph from scanning electronic microscope (SEM) and mineralogy analysis from XRD. The SEM and XRD analyses confirmed that most of the OSA consisted of angular geometric particles. It is also apparent that the OSA is composed of various-sized particles ranging from several to dozens of ultrafine micrometers. Additionally, the microstructure of the OSA has a slightly little amorphous hollow.

Table 4 gives the chemical composition of the OSA. There is mainly calcite which is a white and colourless mineral consisting of calcium carbonate as well as silicon and minor other minerals, such as aluminum, ferrite, sodium, titanium, sulfate, and periclase.

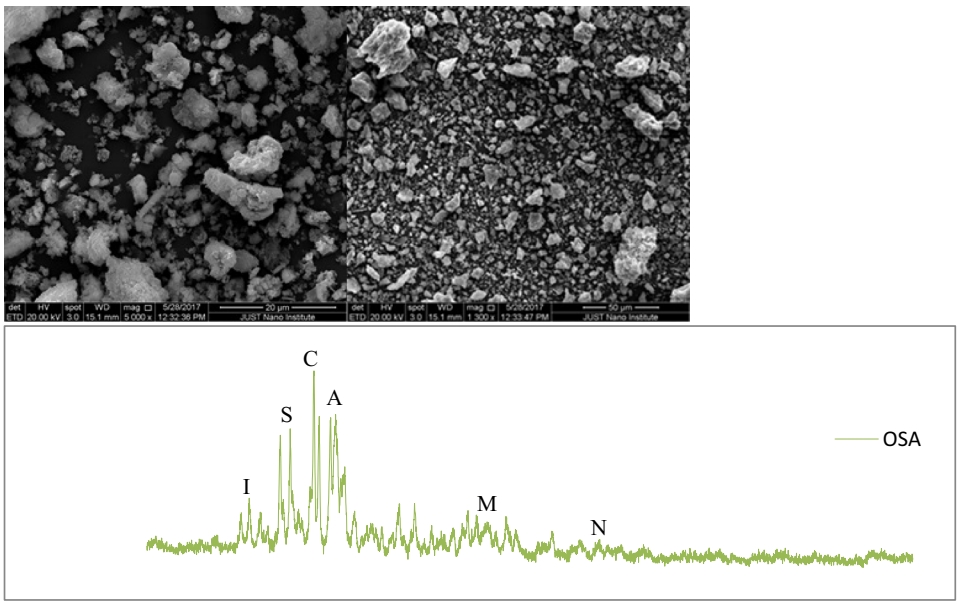

Fig. 4 SEM micrograph and XRD analysis of the OSA used in the current study—C: calcium oxide, S: silicon dioxide, A: aluminum oxide, I: ferrite oxide, M: magnesium oxide, N: sodium oxide

Table 4 The chemical composition of the oil shale ash (OSA)

Type of supplementary cementitious material	Chemical composition (%)									Blaine fineness
	SiO_2	Al_2O_3	Fe_2O_3	CaO	MgO	SO_3	K_2O	TiO_2	Loss in ignition	
Oil shale ash	19	6	2	47	0.8	8	0.6	0.2	5.4	550 kg/m^3

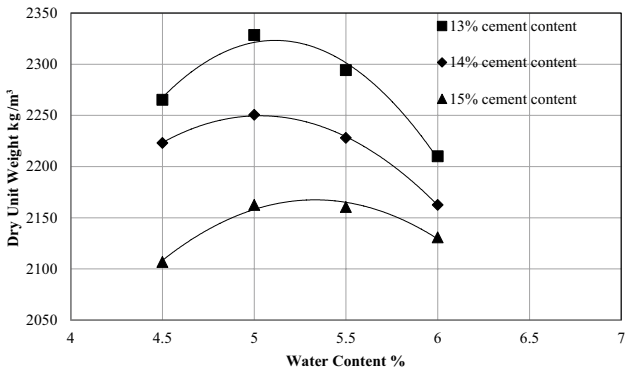

Fig. 5 Dry density–water content curve with different cement content

According to the high calcium oxide (CaO) content of the OSA used, this study classified it as a latent hydraulic additive. Moreover, since the OSA consists of the content of silicon dioxide, aluminum oxide, iron oxide, and calcium oxide with a total of 74%, as well as titanium oxide, this study suggests that the OSA can be accepted as supplementary cementitious material (Table 3, Figs. 3, 4).

2.2 Mix Proportions of RCC

In this study, the mix proportions of the RCC were calculated according to the method of soil compaction, which is based on a current relationship between the moisture content and the dry density of the RCC. For this research, the water:binder ratio (w/b) was kept constant at 0.4 for all RCC mixes. The cementitious materials content for RCC pavement generally ranged from (11–17%) by mass of dry aggregate according to ACI 211.3R [25]. So in this research three different cement of 13%, 14%, and 15% and different water content of 4.5%, 5%, 5.5%, and 6% were considered to obtain the optimum moisture content (OMC) that corresponds with the highest unit weight. It is clear from Fig. 5 that the OMC occurred at 13% cement content with 5.1% water content and w/c of 0.4. Table 5 shows the groups and mix proportions of RCC.

2.3 Mixing, Casting, and Curing of RCC Specimens

A tilting drum mixer with a volume of 0.15 (m^3) was used in the mixing procedure. RCC components were mixed according to the following steps; (1) a little amount of water was poured into the mixer; (2) the coarse aggregates were added; (3) the cement and fine aggregate were then added gradually; (4) the water reducer was incorporated at various percentages by cement weight to provide sufficient workability; (5) the constituents were blended for about 6 min in the mixer to obtain such cohesive RCC mixes. After mixing, the fresh constituent materials of the RCC were cast in three layers and compacted according to the ASTM C 1435 [60] by a vibrating compaction hammer, with a minimum power input of 900 (W) and the ability to provide at least 2000 impacts per minute. After casting, the specimens were covered with wetting burlap for 24 h to prevent moisture content loss. After 24-h, RCC specimens were moved and cured in water tanks until the day of testing. Specimens were tested at 7-days, 28-days, and 90-days of casting.

Table 5 Mix proportion of RCC

Types of mixing		Mixing constituent proportion as kilogram per cubic meter							Ratio of mixing feature	
		Cement	Aggregate		Silica sand	Water	OSA	Water reducer (WR)	w/b	OSA/C
			CA > 4 (mm)*	FA < 4 (mm)*						
RCC	O-0%	266	924.6	1073	57.2	102.75	0	3.25	0.4	0
	O-10%	239.4	924.6	1073	57.2	102.75	26.6	3.72	0.4	0.1
	O-20%	212.8	924.6	1073	57.2	102.75	53.2	4.25	0.4	0.2
	O-30%	186.2	924.6	1073	57.2	102.75	79.8	4.78	0.4	0.3
	O-40%	159.6	924.6	1073	57.2	102.75	106.4	5.32	0.4	0.4

*The CA stands for coarse aggregate and the FA stands for fine aggregate

2.4 Testing Procedures and Standards

2.4.1 Physical Properties

2.4.1.1 Density of Fresh and Hardened Concrete The fresh density of RCC mixes with different OSA replacement ratios was measured according to the specification in ASTM C138 / C138M-09 [61] while the hardened density of the RCC specimens was measured according to ASTM C642-13 [51] standards.

2.4.1.2 Porosity Measurement The porosity of all mixes was measured according to ASTM C642-13 [62]. The porosity is defined as the ratio of the volume of voids to the total volume of the concrete mass. All specimens were oven-dried at 105 ± 5 °C at the age of 90 days, and then they were left to cool up to room temperature. The porosity of RCC was measured at the age of 90 days according to Eq. (1).

$$P = \left(1 - \left(\frac{W_1 - W_2}{V * q_w}\right)\right) * 100\%, \quad (1)$$

where the P is the total porosity of the RCC (%), W_1 is the mass of the specimen underwater (kg), W_2 is the oven-dried mass, V is the volume of the specimen (cm^3), and q_w is the density of water (1000 kg/m^3).

2.4.1.3 Ultrasonic Pulse Velocity (UPV) The UPV device used is shown in Fig. 6, the device has two metalheads; a transmitter and a receiver that are connected to a control panel. The UPV device measures the time that a wave needs to travel from the transmitter to the receiver through the concrete.

The UPV readings were taken indirect methods for each two opposite sides of cubes at each 32 cycles as shown in Fig. 7.

Fig. 6 Ultrasonic pulse velocity (UPV)

Fig. 7 UPV direct test

2.4.2 Mechanical Properties

In this research, cylindrical steel molds of 150 (mm) diameter and 300 (mm) height were used for testing the compressive and splitting tensile strength. Whereas cubic steel molds of 150 × 150 × 150 (mm) dimensions were used for testing the freezing and thawing effect and the weight loss after freezing and thawing cycles. In addition, prism steel molds of 100 × 100 × 300 (mm) dimensions were used for testing the flexural strength. The compressive stress and the splitting tensile stress of the cylinders were determined according to the standards of ASTM C 39 [63] and ASTM C 496 [64], respectively. The compressive stress was determined at 7 days and 28 days of casting. The flexural strength was evaluated according to ASTM C 293 [65]. The modulus of elasticity was measured at the age of 90-days according to ASTM C 469 [66]. The stress–strain relationship was obtained using LVDT. Then, the modulus of elasticity is calculated based on the relationship between the stress and the strain in the linear part.

2.4.3 Durability Measurement

The freeze–thaw cycle resistance of hardened RCC was determined using 150 (mm) cubes according to ASTM C666/C666M standards [67]. Loss in weight of the RCC was measured after the freezing–thawing cycle using the following equation:

$$W = \left[\left(W_2 - W_1\right)/W_1\right] * 100, \quad (2)$$

where W is the loss in weight (%), W_1 is the initial weight of specimens before the freeze–thaw cycles, and W_2 is the weight of specimens after n cycles. Also, the compressive stress of the specimens of RCC with different replacements of cement with OSA was measured after 300 cycles.

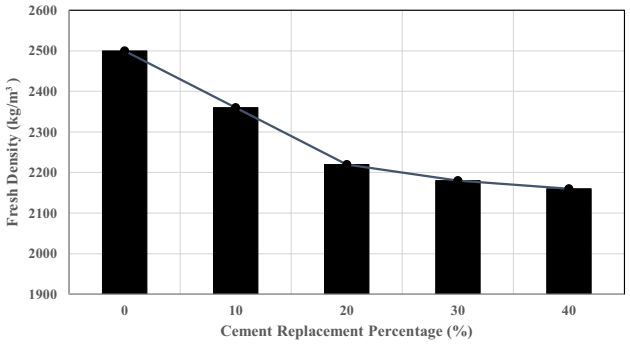

Fig. 8 The change in the fresh density for RCC mixes with different replacement percent of the OSA with cement

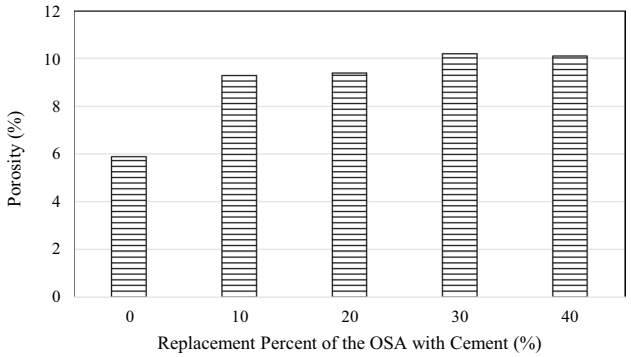

Fig. 9 The Porosity of RCC, at the age of 90 days curing

2.4.4 Microstructure and Mineralogical Phase Analysis

To observe the chemical compound in the hardened inner structure of the RCC at 90 days, a current scanning electron microscopy was used according to the ASTM C1723-16 standard [68]. To analyze the proportion of mineral phase in the RCC at 3, 14, and 90 days, the study uses the X-Ray Powder Diffraction (XRD) according to ASTM C1365-18 standard [69]. The mineralogy of the RCC was evaluated regarding the rules of both Bragg's law and the ASTM C1365-18 standards [68].

3 Results and Discussion

3.1 Physical Properties

3.1.1 Density of Fresh Mixing

Figure 8 shows the fresh density of RCC mixes with different replacement levels. Using oil shale ash as a replacement for cement has decreased the fresh density as shown in Fig. 8. This reduction reached the lowest quantity in the mixing of O-10%. As 10% OSA was replaced with cement, the reduction equals 3% in the fresh density. The highest reduction in the fresh density of RCC is determined in the mix O-40%, containing 40% OSA replacement of cement, as it equals 13.6%. The fresh density of RCC mix O-20% is approximately the same as the fresh density of mixes O-30% and O-40%. Moreover, increasing the OSA content leads to a decrease in the density of fresh RCC. This reduction can be attributed to the smaller specific gravity of OSA (2.69) compared to cement (3.19). This reduction in the unit weight can be desirable for paving structures such as concrete bridges and concrete blocks. The reduction in unit weight reached 13.6% as of the control specimen.

3.1.2 Porosity

Figure 9 shows the porosity of RCC mixes. All mixes containing OSA had higher porosity than OSA-free mix. The increase in porosity of RCC with OSA reached the lowest quantity in the mixing of O-10%. As the 10% OSA is replaced with cement, the increase in porosity equals 51%. The highest increase in the porosity of RCC is recorded at 30 and 40% OSA replacement with cement, which equals 63.5%. It can be seen that the porosity increased with the decrease in density as the OSA content increased. This can be explained due to the high absorption of the OSA. Therefore, less water will be available which could react with cementations materials. Hence, the use of OSA will reduce the hydration process at a constant water/cement ratio. Thus, the percentage of voids will increase. This agrees with the results of Raado et al. [70], who reported that the existence of free CaO and SiO_2, causes water demand due to the hydration process. This means the higher the water demand, the higher the volume of large capillary pores; therefore, it could increase the percentage of porosity.

The results complied well with the results of existing calcium oxide (CaO) and silicon dioxide (SiO_2) that caused the porosity based on water demand in the hydration process of the binder. The higher the water demand, the higher the volume of large capillary pores. However, the use of OSA had increased the porosity ratio within the acceptable [37, 38, 71, 72]

3.2 Mechanical Properties of RCC with OSA

3.2.1 Compressive Strength

The compressive strength was determined by testing standard cylinders (150 × 300 mm) at 7 and 28 days. Each test was carried out on three cylinders for each curing day. Figure 10 and Table 6 show the compressive strength at the 7th-day and 28th-day for the RCC with different OSA replacement

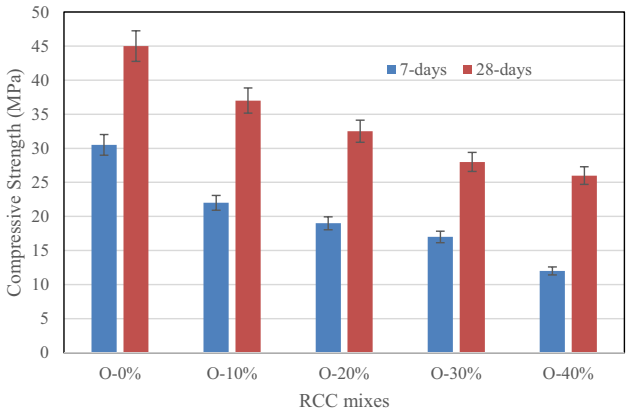

Fig. 10 The compressive strength at 7th day and 28th day for the RCC, and the substitution percent of the oil shale ash for cement

levels of cement. The compressive strength was between 12 and 22 MPa at the age of 7 days, and between 26 and 37 MPa at the age of 28 days. This means that this could be referred a success for using oil shale ash as a supplementary latent hydraulic cementitious material in the RCC. In a study by Uibu et al. [8] for oil shale ash backfilling in concrete, and its strength development, the compressive stress was between 1 and 5 (MPa) at 7 days, and the 28 days compressive stress reached a maximum value of 25 MPa. As seen in Fig. 10, the compressive strength decreased by increasing the OSA content. For example, the compressive strength reached 37, 32.5, 28, and 26 at 28 days of curing for 10%, 20%, 30%, and 40% OSA replacement content, respectively. The reduction in strength reached 17.8%, 27.8%, 37.8%, and 42.2% for 10%, 20%, 30%, and 40% OSA replacement, respectively. The reduction in compressive stress can be attributed to the absence of an activator for the calcium oxide (CaO) in the chemical composition of the OSA (Table 3).

Also, the reduction in strength of RCC upon replacement with OSA can be attributed to the decrease in the cement, siliceous, and calcareous contents which are responsible for the cementing and strength properties [10, 73]. Ashteyat et al. [15] reported a decrease in strength of 48% at 30% OSA replacement, for self-compacted concrete, while Meddah [9] reported a decrease in strength of 30.5% at 40% OSA replacement.

According to the ACI.325.10-95, the minimum compressive stress for the roller compacted concrete which would be used for the public traffic depends on the pavement layer [27]. The minimum recommended strength is 27.6 MPa at 28 days of curing for the construction of RCC pavements (as a surface layer) as specified by [27]. However, the 28 days' compressive strength of O-10%, O-20%, and O-30% of RCC is greater than a number of data reported in RCC in situ applications [27]. Also, O-10%, O-20%, and O-30% RCC satisfied the criteria of ACI [27] as well. Therefore, the study could suggest the mixing of the O-10%, the O-20%, and the O-30% as an upcycling example of the OSA in the RCC mixing.

A study published by Radwan et al. [74] supports the aforementioned inferences in the current study. They agree with the inference that the OSA is an essential activator for the RCC since it has plenty of chemical compounds such as calcium oxide, silicon dioxide, aluminum oxide, ferrite oxide, and titanium oxide. Therefore, they used an alkali activator for the blended cement containing oil shale ash, and in the absence of an alkali activator, the blended cement containing OSA showed nearly 20% lesser compressive stress than that of the Portland cement. With an alkali activator, the compressive stress of cement blended OSA increased the same as in Portland cement [74].

3.2.2 Splitting Tensile Stress

Figure 11 and Table 6 show the splitting tensile stress results of RCC with different OSA replacement ratios. The splitting tensile stress reflects the ability of concrete to resist the tension force since the concrete is a brittle material and it will not be able to face the tensile force significantly. The results indicate that the splitting tensile strengths were in the range of 2.1–4.1 MPa at the age of 28 days. The splitting tensile stress of the RCC reached the highest quantity at the age of 90 days in standard water curing, 4.1 (MPa), because it includes 100% cement content. It is clear that when OSA content increases, the splitting strength

Table 6 Results of mechanical properties of RCC

Mixes	Compression strength (MPa)		Splitting strength (MPa)			Flexural strength (MPa)			Modulus of elasticity (GPa)
	7 days	28 days	7 days	28 days	90 days	7 days	28 days	90 days	90 days
O-0%	30.5	45	3	4.1	4.45	6.4	8.5	10	38.1
O-10%	22	37	2.4	2.7	3	5.8	8.1	9.7	21
O-20%	19	32.5	2	2.6	2.7	4.2	5.9	6.3	18.2
O-30%	17	28	1.8	2.4	2.6	4.1	5.8	6.1	17.2
O-40%	12	26	2	2.1	2.6	3.6	3.7	3.9	13.4

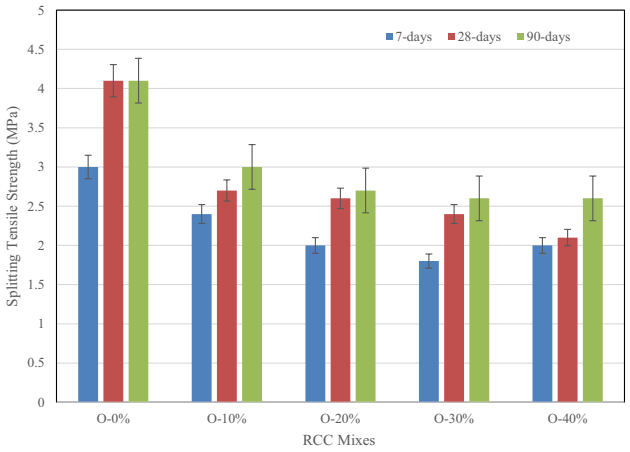

Fig. 11 The change in the splitting tensile stress of the RCC

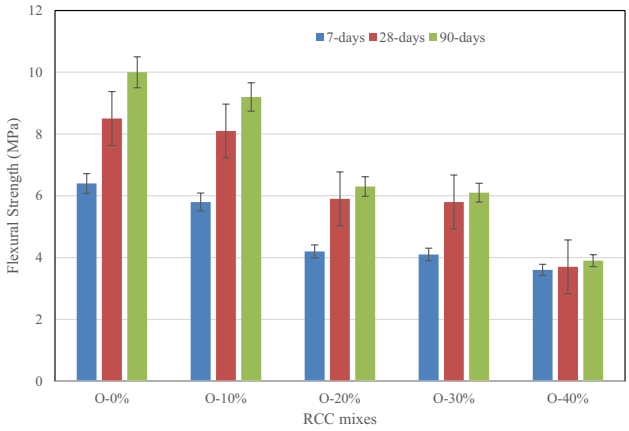

Fig. 12 The flexural strength at 7th day and 28th day and 90th-day for RCC and the substitution percent of the oil shale ash for cement

decreases. The splitting strength reached 4.1 MPa for the control mix at 90 days of age while it reached 3, 2.7, 2.7, and 2.6 MPa for 10%, 20%, 30%, and 40% OSA content. The reduction reached a minimum value of 26.83% at 10% OSA replacement, and a maximum value of 36.6% at 40% OSA replacement. Hesami et al. [38] reported a splitting strength between 2.18 and 3.3 for RCC with coal waste and limestone powder as partial replacements for cement, while Debbarma et al. [32] and Settari et al. [37] reported RCC with a splitting strength of 1.6–2.6 MPa for RCC with recycled asphalt and high cement content. Also, some of the data reported in a number of RCC in-situ applications showed a splitting tensile strength of 2.7–3.1 MPa [27]. At 7 and 28 days, the splitting tensile stress of O-10% RCC is greater than that of in-situ applications of RCC used in the projects of Barracks and Campbell [27].

The reduction of splitting strength in RCC with OSA shows the same trend for a decrease in compressive strength. According to the guideline of RCC, the tensile strength at the age of 28 days for RCCP are generally, 2–4 MPa [75]. All, the splitting tensile strength is above 2 MPa and satisfies the required criteria for class 2 pavement concrete according to [76, 77].

3.2.3 Flexural Strength

RCC must be designed to withstand high flexural loads and repeated loads, such as trucks and cars in RCC pavement applications, and a heavy water load as being in the RCC dams without failure. Figure 12 and Table 6 show the flexural stress at 7, 28, and 90 days of all RCC mixes.

The flexural strength of RCC reached the highest value at the ages of 7, 28, and 90 days in standard water curing, 6.4 (MPa), 8.5 (MPa), and 10 (MPa), respectively. The reduction of flexural strength of RCC reached the lowest value in the mixing of O-10%. As the 10% OSA was replaced with cement, the reduction equals 10%. The highest reduction in the flexural strength of RCC was at 40% OSA replacement with cement which equals 43.7%. At 7 days, the flexural strength of O-20% of RCC approximately equals the flexural strength of O-30% of RCC. The mixing of O-40% of RCC demonstrated 10.5% lesser 7 days flexural strength when compared to the mixing of O-20% and O-30% of RCC. The 7 and 28 days flexural strength of O-10% and O-20%, and O-30% of RCC was greater than some of that of in-situ applications of RCC reported in [27]. Fakhri and Saberik [54] the flexural strength of RCC with silica fume was between 5 and 7 MPa depending on the rubber content. Also, Fakhri and Amoosoltani [55] reported a flexural strength range from 2 to 8.8 MPa depending on the cement content and the amount of rubber and recycled asphalt aggregate used in RCC. Boussetta et al. and Debbarma et al. [32] reported a flexural strength between 2 and 3.5 MPa. Rahmani [36] reported a flexural strength of 5.6–8.5 MPa depending on the water-cement ratio. İn a study by [56] the flexural strength was 4.2–5.16 MPa depending on the amount of fly ash replacement of cement.

According to Portland Cement Association (PCA), the flexural strength ranges from 3.5 to 7 MPa at 28 days [47, 57, 64]. As it can be seen from Fig. 12, all RCC mixes reached a flexural strength higher than 3.5 MPa, which clearly indicates that RCC with OSA as a replacement of cement up to 40% can be suitable for pavement applications.

3.2.4 Modulus of Elasticity

Figure 13 and Table 6 show the stress–strain curves of RCC with different OSA replacement percentages of cement. The modulus of elasticity was measured at 90 days of casting.

The curves in Fig. 13 show two stages. The first one is a linear behavior stage, then it is followed by a non-linear

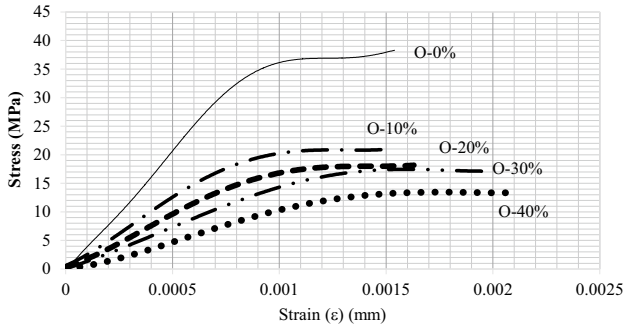

Fig. 13 Stress–strain curves for the RCC, at various replacement percent of OSA with cement

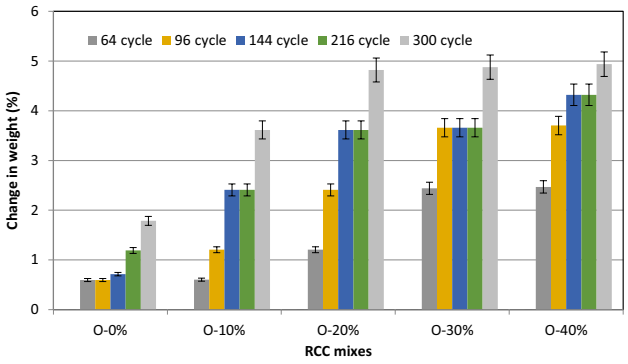

Fig. 14 The loss in weight after freezing and thawing cycles for RCC with different OSA replacement levels

behavior stage due to the brittle behavior of RCC. As the OSA replacement content increased, the linearity in the stress–strain diagram decreased. It provides nonlinearity for the RCC with OSA through a relatively low-stress gain. The decrease in linearity with increasing the OSA replacement level is due to the decrease in the ultimate flexural strength which also relates to the reduction in modulus of elasticity. In addition, increasing the OSA content in the specimens of RCC provides much more ductility. On the other hand, it was observed, in the experiment, that the specimen of the O-40% does not have an obvious crack on its surface until failure.

The modulus of elasticity of the control RCC mix reached the highest value at the age of 90 days because it includes 100% cement content. The reduction in modulus of elasticity reached the lowest percentage in the O-10% mix as the 10% OSA was replaced with cement, this reduction equals t1%. The highest reduction in the modulus of elasticity was recorded for 40% OSA replacement with cement, and it equals to. At 90 days, the modulus of elasticity of O-20% of RCC reached the same modulus of elasticity of O-30% RCC mix.

3.3 Durability Properties of RCC with OSA

3.3.1 Freezing and Thawing

The 38-day freeze–thaw cycle resistance of the hardened RCC with different OSA replacement levels was determined. In the freezing–thawing cycle, the loss in weight was measured after the cycle of 0th, 64th, 96th, 144th, 216th, and 300th, and the loss in the compressive stress was determined at the 0th, 144th, and 300th cycle also, UPV reading was taken after 0, 96,144, 216 and 300 freeze–thaw cycles.

3.3.2 Change in Weight After Freezing–Thawing Cycle

The adequacy resistance of frost attack in the RCC with different OSA content can be determined by freezing and thawing tests. ASTM has developed two tests for frost resistance in concrete material. In both of these, rapid freezing is applied, one of them freezing and thawing takes place in the water while the other freezing in air and thawing in water. This study used the freezing and thawing method specified by the ASTM to determine the effect of frost exposure in the RCC. Figure 14 shows the loss in weight after freezing and thawing cycles.

It is clear that the weight decreased when the number of freezing–thawing cycles and OSA replacement levels increased, this is due to the increase in the water absorption of OSA which means more capillary pores lead to higher water pressure during the freezing process and an increase in weight loss in the RCC with different OSA replacement level. The loss in weight of RCC reached the lowest quantity in the mixing of O-10%. At 10% OSA replacement of cement, the reduction equals 3.6% only. But in all mixtures, the change in weight after freezing–thawing was not significant, the maximum weight loss was 5% for a mixture with a 40% OSA replacement level [50–53]. Figure 15 shows the damages which happen to the RCC specimen due to freezing and thawing.

3.3.3 Compressive Strength After Freezing–Thawing Cycle

Figure 16 shows the compressive strength of all specimens after a number of freezing and thawing cycles. The compressive strength decreased with increasing the number of freezing and thawing cycles and OSA content. A significant reduction in compressive strength was noticed after 144 freezing and thawing cycles. The decrease in the compressive strength can be explained as the porosity increase with increasing OSA content, the volume of freezable water in the cement paste will increase and cause internal expansive pressure during freezing. This will increase the cracks and weight loss in the specimens of RCC. The reduction in the compressive strength of RCC reached the lowest quantity in

Fig. 15 Freezing and thawing damages for RCC specimens after 300 cycles

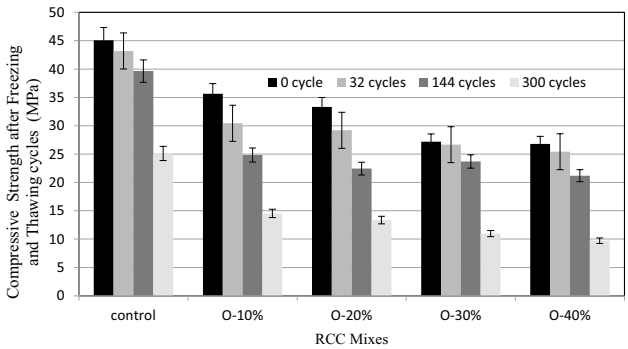

Fig. 16 Compressive strength vs. OSA content at different freezing and thawing cycle

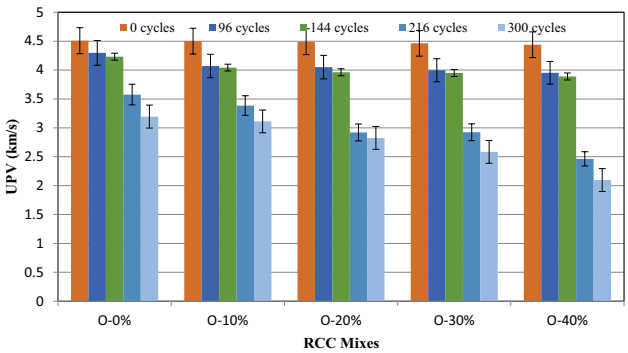

Fig. 17 Ultrasonic pulse velocity (UPV) for RCC mixes specimens at different F/T cycles

the mixing of 0% OSA, the reduction was 44%. As the 10% OSA is replaced with cement, the reduction equals 59%. The highest reduction in the compressive stress of RCC was recorded for the O-40% mix. Ghahari [51] reported a decrease in strength of 35% for RCC with fly ash, while [50] reported a decrease of 10% for high strength RCC.

3.3.4 Ultrasonic Pulse Velocity (UPV) Result for RCC with OSA Mixtures

The ultrasonic pulse velocity method is a non-destructive test (NDT) of concrete. It is used to establish the quality and homogeneity of the concrete in relation to specific standard requirements. Also, UPV is used to detect changes in the concrete structure caused by corrosion, cracks, voids, and other imperfections. In this study, ultrasonic pulse velocity was measured after 0, 96,144, 216, and 300 freeze–thaw cycles at the center of the cube's faces through a direct path length of 150 mm.

Figure 17 shows the average pulse velocity of three cubical specimens for each RCC mix. It can be noted that the reference UPV (before any freeze–thaw cycle) values for all RCC mixtures were between 4.44 and 4.51 km/s, the range corresponds to strong and good concrete [78, 79].

As noted from the previous figure, The UPV readings of RCC cubic specimens before freeze and thaw cycles showed that the maximum UPV value was obtained for the control mixture with a value of 4.51 km/s. The minimum value was 4.40 km/s for 40% OSA replacement. The UPV for 10%, 20% and 30% OSA replacement mixtures reached 4.5, 4.49 and 4.46 km/s, respectively. The UPV values decreased by increasing the replacement ratio of OSA. Compared to the control mixture, there was a 2.4% decrease in UPV values for 40% OSA mixtures. The decrease in UPV readings was noticed after 144 cycles. The UPV readings after 216 cycles of freeze–thaw were: 3.57, 3.38, 2.92, 2.92 and 2.46 km/s for control, 10%, 20%, 30%, and 40% OSA replacement mixtures, respectively. The quality of concrete refers to good quality for control mixtures, while it was intermediate for O-10%, O-20%, and O-30% [79].

3.4 Microstructure Analysis of RCC

3.4.1 Mineralogical Phase Analysis with XRD

This study conducted the X-Ray diffraction (XRD) analysis for the RCC specimen containing 20% OSA at the ages of 3, 14, and 90 days. The results are reported in Fig. 18.

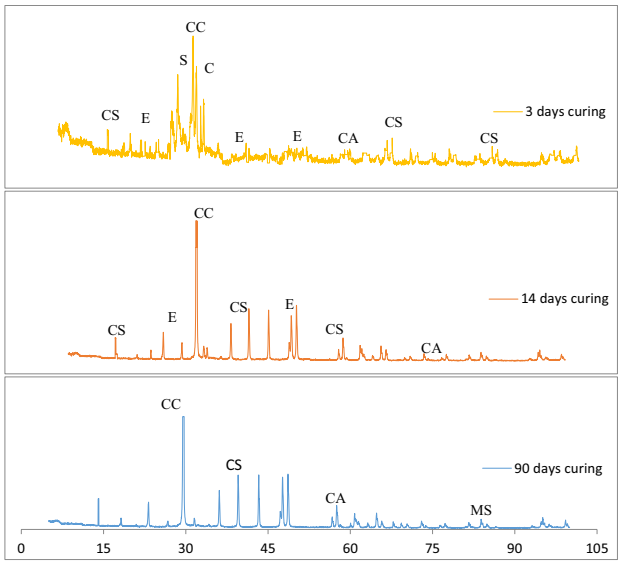

Fig. 18 The XRD analysis for O-20% specimen at the curing ages of the 3th-day, 14th-day, and 90th-days. *CC* Calisum, *E* Ettrengite, *S* SiO_4, *C* CaO, *CS* Ca_2SiO_4

At 3 days, the content of the calcite ($CaCO_3$), calcium oxide (CaO), silicon dioxide (SiO_2), and calcium-silica-hydrate (C-S–H) was found to be major compounds as well as the minor compound content of ettringite and calcium-aluminate-hydrate (C-A-H) in the O-20% paste.

OSA hydration involves anhydrite conversion to gypsum and the formation of ettringite. The ettringite is formed in RCC with OSA. Ettringite was found mainly because these OSA contain sulfates [8, 9, 12, 16]. The ettringite formation depends on the availability of dissolved sulfates and supports cementation in the early phase of hardening because its needle-like structure leads to crystal interlocking [9]. Sulfate reacted with calcium aluminate hydrates of ash to form ettringite at the early age of the mixture according to the following equation [8, 12, 16]

$$CaSO_4 + 2H_2O \rightarrow CaSO_4.2H_2O, \tag{5}$$

$$3Ca(OH)_2 + 2Al(OH)_3 + 3CaSO_4 + 26H_2O \rightarrow Ca_6Al_2(SO_4)_3(OH)_{12}.26H_2O. \tag{6}$$

Except for the calcium oxide content, at 14 days, it was analyzed that there were the same major-minor compounds in the O-20% of RCC paste. There was a difference between the major compound and minor compound in the O-20% of RCC paste at 90 days. This difference is due to the magnesium silicate ($MgO{\cdot}SiO_2{\cdot}H_2O$) hydrate (M-S-H). At 90 days in the O-20% of RCC paste, all other major and minor compounds were similar to the major and minor compounds of the O-20% of RCC paste at 3 and 14 days.

The mineral composition in the O-20% of RCC paste is due to the chemical composition of OSA. The chemical composition of OSA has a high quantity of silicon dioxide (SiO_2) and calcium oxide (CaO) as well as the oxide of aluminum and ferrite which are very important compounds in the hydration reaction of cement to turn out new hydration products, such as calcium-aluminum-hydrate (Fig. 18). It is clear to infer that the oxide of silicon would be consumed by the calcium hydroxide (CH) which is the greatest hydration product of cement to form calcium-silicate-hydrate (Fig. 18). This leads to the increase in the demand for water and output of delayed ettringite formation which decreases the strength gain and increases the expansion and failure based on a crack in the RCC. The increase in the water absorption of the OSA leads to an increase in the water demand of the RCC. Therefore, this study used a water reducer to prevent being unhydrated cement particles which results in decreasing the stress gain [8, 32].

3.4.2 Microstructure Analysis with SEM

The SEM micrographs in Fig. 19 showed ettringite which was increasing with increasing the OSA content. The ettringite is formed in the early age of concrete material to reduce the flash setting of cement, but it is forming at a later age. This means that the hydration of cement has not been completed, which will lead to expansion. Therefore, it weakened the concrete material. It was observed that in the hydration of cement with OSA, angular cement grains were surrounded by radiating fibers of calcium silicate hydrate (C-S-H) resembling the pattern of C-S-H of ordinary cement. Randomly oriented portlandite (CH) crystals and prismatic ettringite crystals were widely dispersed through the paste of O-10%, O-20%, O-30%, and O-40%. However, in the O-40% at the curing age of 90 days, it was found that the OSA grains were covered with amorphous (with respect to C-S-H) layered CH hydration products. The matrix phase is mainly composed of short radicular outgrowths of C-S-Hs around cement grains and needle-shaped ettringite crystals (Fig. 19). The microstructure of hydrated paste of RCC at the curing age of 90 days was presented by amorphous gel filling spaces between hydrated particles.

In RCC with OSA, layered accumulations of the CH crystals of about 12 µm in width are intermingled through the paste. There is visible densification around the ordinary cement grain due to partial hydration of the OSA grain, leading to the formation of additional C-S-H. At the curing age of 90 days, the OSA grains were well located in the matrix and were sunk in a layered CH. Observation of paste based on the RCC with OSA demonstrated

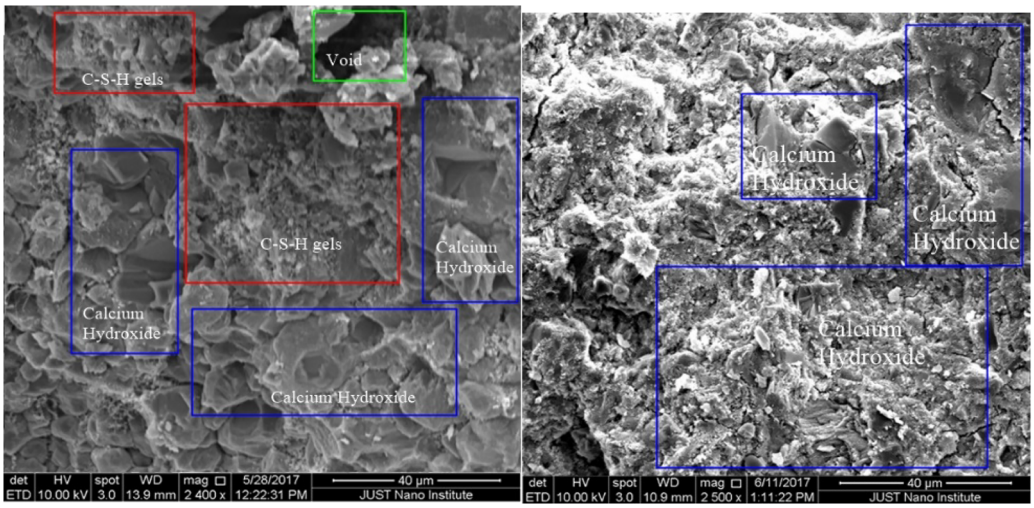
C-S-H gels
Void
C-S-H gels
Calcium Hydroxide
Calcium Hydroxide
Calcium Hydroxide
Calcium Hydroxide
Calcium Hydroxide
Calcium Hydroxide
Calcium Hydroxide
det HV spot WD mag 5/28/2017 40 µm
ETD 10.00 kV 3.0 13.9 mm 2 400 x 12:22:31 PM JUST Nano Institute
det HV spot WD mag 6/11/2017 40 µm
ETD 10.00 kV 3.0 10.9 mm 2 500 x 1:11:22 PM JUST Nano Institute

(a) (b)

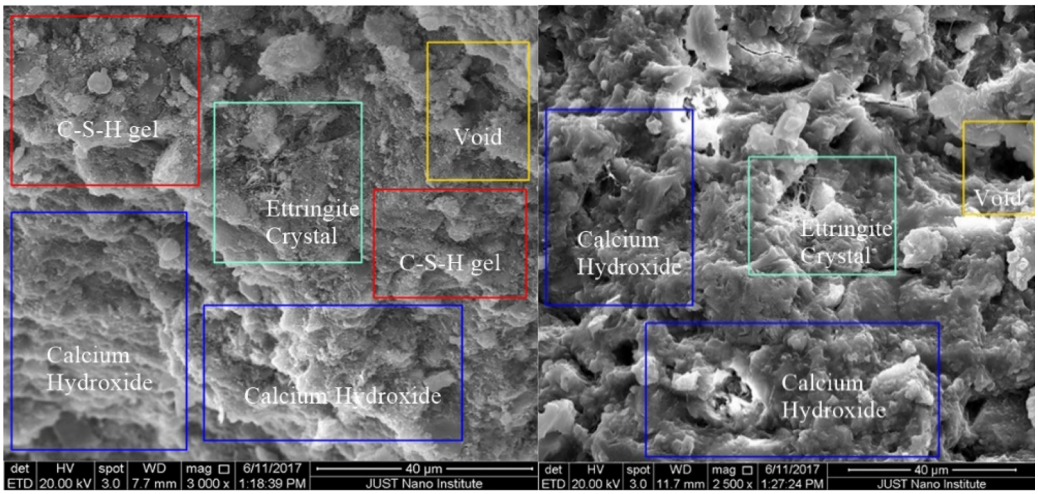
C-S-H gel
Void
Ettringite Crystal
C-S-H gel
Calcium Hydroxide
Calcium Hydroxide
Calcium Hydroxide
Ettringite Crystal
Void
Calcium Hydroxide
det HV spot WD mag 6/11/2017 40 µm
ETD 20.00 kV 3.0 7.7 mm 3 000 x 1:18:39 PM JUST Nano Institute
det HV spot WD mag 6/11/2017 40 µm
ETD 20.00 kV 3.0 11.7 mm 2 500 x 1:27:24 PM JUST Nano Institute

(c) (d)

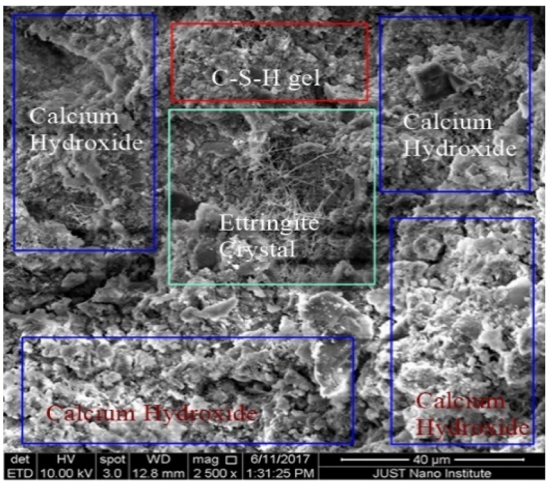
Calcium Hydroxide
C-S-H gel
Calcium Hydroxide
Ettringite Crystal
Calcium Hydroxide
Calcium Hydroxide
det HV spot WD mag 6/11/2017 40 µm
ETD 10.00 kV 3.0 12.8 mm 2 500 x 1:31:25 PM JUST Nano Institute

(e)

◂**Fig. 19** The SEM micrographs for RCC at curing age of 90th-day; SEM image of O-0% (**a**), SEM image of O-10% (**b**), SEM image of O-20% (**c**), SEM image of O-30% (**d**), SEM image of O-40% (**e**)

that the OSA grains turned out as amorphous reaction prisms. In the CH phase, the matrix of RCC with OSA was found to be richer in calcium than that of the paste of 0% OSA RCC. At the age of 90 days, the microstructure of RCC with OSA was further densified with respect to RCC paste.

4 Conclusions

An experimental program was conducted to investigate the durability and mechanical properties of RCC mixes containing oil shale ash (OSA) as a partial replacement for cement. Based on the experimental results, the following conclusions could be drawn:

- As the OSA content increases, the density of the RCC mixture decreases since OSA has lower specific gravity than cement which leads to reduce the total weight.
- As the OSA content increases, the mechanical properties of RCC specimens decreases. The decrease in the mechanical properties of RCC specimens' reached more than 10%.
- On average, the RCC mix containing 10% OSA showed higher compressive strength, splitting strength, flexural strength, and modulus of elasticity compared to the RCC mixes containing higher OSA content. Therefore, to use OSA without a significant effect on the RCC mixture characteristics, an optimum content of 10% of OSA can be used to obtain close strength values to the control mix.
- All mixes reached a compressive strength greater than 27.6 MPa, except the mixture with a 40% OSA replacement level. Based on the experimental results, it is possible to use waste OSA in producing RCC for up to 30% as a main base coarse.
- Based on the results of freezing and thawing cycle tests, and UPV, all mixes with OSA showed a remarkable reduction after 216 freeze–thaw cycles. Besides, all specimens showed a decrease in weight and compressive strength, especially after several cycles of freezing and thawing.

Acknowledgement The authors wish to acknowledge the financial support provided by the deanship of research at Jordan University of Science and Technology via a research grant, (number 112/2017). The authors wish to acknowledge the assistance of the technicians at the civil engineering laboratories.

Declarations

Conflict of interest The authors declare no conflict of interest.

References

1. Aprianti, E., Shafigh, P., Bahri, S., & Farahani, J. N. (2015). Supplementary cementitious materials origin from agricultural wastes a review. *Construction and Building Materials, 74*, 176–187. https://doi.org/10.1016/j.conbuildmat.2014.10.010
2. Celik, K., Jackson, M. D., Mancio, M., Meral, C., Emwas, A.-H., Mehta, P. K., et al. (2014). High-volume natural volcanic pozzolan and limestone powder as partial replacements for Portland cement in self-compacting and sustainable concrete. *Cement and Concrete Composites, 45*, 136–147. https://doi.org/10.1016/j.cemconcomp.2013.09.003
3. Mirza, J. (2019). Reduction in ecology, environment, economy and energy in concrete industry using waste materials. In M. S. Kırgız (Ed.), *The proceedings of abstracts book of the third annual international conference on eco-sustainable construction materials* (August 26–29, 2019, p. 16), İstanbul, TR. ISBN: 978-605-031-179-2.
4. Dabbas, M. A. (1997). Oil shale: hopes and ambitions (in Arabic). In *Second Jordanian conference for mechanical engineering, JIMEC '97*. Amman-Jordan, JAE.
5. Haddad, R. H., Ashteyat, A. M., & Lababneh, Z. K. (2018). Producing geopolymer composites using oil shale ash. *Structural Concrete*. https://doi.org/10.1002/suco.201800007
6. Sharo, A. A., Ashteyat, A. M., Alawneh, A. S., & Bany Khaled, B. A. (2018). The use of oil shale fly ash to improve the properties of Irbid soil. *World Journal of Engineering*. https://doi.org/10.1108/wje-10-2017-0325
7. Bourdot, A., Thiéry, V., Bulteel, D., & Hammerschlag, J.-G. (2016). Effect of burnt oil shale on ASR expansions: A petrographic study of concretes based on reactive aggregates. *Construction and Building Materials, 112*, 556–569. https://doi.org/10.1016/j.conbuildmat.2016.02
8. Uibu, M., Somelar, P., Raado, L.-M., Irha, N., Hain, T., Koroljova, A., & Kuusik, R. (2016). Oil shale ash based backfilling concrete—Strength development, mineral transformations and leachability. *Construction and Building Materials, 102*, 620–630. https://doi.org/10.1016/j.conbuildmat.2015.10
9. Seddik Meddah, M. (2015). Durability performance and engineering properties of shale and volcanic ashes concretes. *Construction and Building Materials, 79*, 73–82. https://doi.org/10.1016/j.conbuildmat.2015.01
10. Raado, L.-M., Haın, T., Lıısma, E., & Kuusık, R. (2014). Composıtıon and propertıes of oıl shale ash concrete. *Oil Shale, 31*(2), 147. https://doi.org/10.3176/oil.2014.2.05
11. Raado, L.-M., Tuisk, T., Rosenberg, M., & Hain, T. (2011). Durability behavior of Portland burnt oil shale cement concrete. *Oil Shale, 28*, 507–515. https://doi.org/10.3176/oil.2011.4.04
12. Usta, M. C., Yörük, C. R., Hain, T., Paaver, P., Snellings, R., Rozov, E., & Uibu, M. (2020). Evaluation of new applications of oil shale ashes in building materials. *Minerals, 10*(9), 765. https://doi.org/10.3390/min10090765
13. Vatin, N., Barabanshchikov, Y., Usanova, K., Akimov, S., Kalachev, A., & Uhanov, A. (2020). Cement-based materials with oil shale fly ash additives. *IOP Conference Series: Earth and Environmental Science, 578*, 012043. https://doi.org/10.1088/1755-1315/578/1/012043
14. Ghannam, S. (2017). The effect of partial replacement of cement by virgin oil shale powder and/or oil shale ash on properties of

cement mortar (comparative study). *Journal of Engineering and Applied Science, 12*, 5281–5285. https://doi.org/10.3923/jeasci.2017.5281.5285
15. Ashteyat, A., Haddad, R. H., & Yamin, M. M. (2012). Production of self-compacting concrete using Jordanian oil shale ash. *Jordan Journal of Civil Engineering, 6*, 202–214.
16. Abdel had, N., & Abdelhad, M. (2018). Characterızatıon and utılızatıon of oıl shale ash mıxed wıth granıtıc and marble wastes to produce lıghtweıght brıcks. *Oil shale, 35*(1), 56. https://doi.org/10.3176/oil.2018.1.04
17. Nov, S., Cohen, H., & Knop, Y. (2020). Treated oil shale ashes as a substitute for natural aggregates, sand, and cement in concrete. *Israel Journal of Chemistry, 60*, 638–643. https://doi.org/10.1002/ijch.202000029
18. Irha, N., Uibu, M., Jefimova, J., Raado, L.-M., Hain, T., & Kuusik, R. (2014). Leaching behaviour of Estonian oil shale ash-based construction mortars. *Oil Shale., 31*, 394–411. https://doi.org/10.3176/oil.2014.4.07
19. Smadi, M. M., & Haddad, R. H. (2003). The use of oil shale ash in Portland cement concrete. *Cement and Concrete Composites, 25*(1), 43–50. https://doi.org/10.1016/S0958-9465(01)00054-3
20. Smadi, M., Yeginobali, A., & Khedaywi, T. (1989). Potential uses of Jordanian spent oil shale ash as a cementive material. *Magazine of Concrete Research, 41*(148), 183–190. https://doi.org/10.1680/macr.1989.41.148.18
21. Attom, M. F., Smadi, M., & Khedaywi, T. (1998). The use of Jordanian oil shale ash as a soil stabilizing agent. *Soils and Foundations, 38*(3), 67–74. https://doi.org/10.3208/sandf.38.3_67
22. Kaljuvee, T., Štubna, I., Húlan, T., Csáki, Š, Uibu, M., & Jefimova, J. (2019). Influence of waste products from electricity and cement industries on the thermal behaviour of Estonian clay from Kunda deposit. *Journal of Thermal Analysis and Calorimetry, 138*, 2635–2650. https://doi.org/10.1007/s10973-019-08319-0
23. Salama, A. H. E. (2022). Effect of grinded oil shale inclusion on some properties of concrete mixtures. *AIP Conference Proceedings, 2440*, 030013. https://doi.org/10.1063/5.0074988
24. M. Al-Hassan, "Behavior of concrete made using oil-shale ash and cement mixtures," (Estonian Academy Publishers, 2006), Vol. 23, No. 2, pp. 135–143
25. Aljbour, S. H. (2016). Production of ceramics from waste glass and Jordanian oil shale ash. *Oil Shale, 33*, 260–271. https://doi.org/10.3176/oil.2016.3.05
26. Gosselin, P., Hrudey, S. E., Naeth, M. A., Plourde, A., Therrien, R., Kraak, G. V., & Xu, Z. (2010). *The Royal Society of Canada Expert Panel: Environmental and health impacts of Canada's oil sands industry* (p. 440). The Royal Society of Canada.
27. ACI. (2001). *State of the-art report on roller compacted concrete pavement*. American Concrete Institute report ACI.325.10-95.
28. Kassem, M., Soliman, A., & Naggar, H. E. (2018). Sustainable approach for recycling treated oil sand waste in concrete: Engineering properties and potential applications. *Journal of Cleaner Production, 204*, 50–59.
29. Schrader, E. K. (2001). Roller compacted concrete for RCC dams—A general overview with comments pertinent to high vs low cementitious content and the cine dam.
30. Lopez-Uceda, A., Agrela, F., Cabrera, M., Ayuso, J., & López, M. (2016). Mechanical performance of roller compacted concrete with recycled concrete aggregates. *Road Materials and Pavement Design, 19*(1), 36–55. https://doi.org/10.1080/14680629.2016.1232659
31. Marchand, J., Gagne, R., Ouellet, E., & Lepage, S. (1997). Mixture proportioning of roller compacted concrete: A review. *Advance Concrete Technology* 457–486 (ACI Special Publication, SP-171).
32. Debbarma, S., Singh, S., & Ransinchung, G. D. R. (2019). Laboratory investigation on the fresh, mechanical, and durability properties of roller compacted concrete pavement containing reclaimed asphalt pavement aggregates. *Transportation Research Record: Journal of the Transportation Research Board*.
33. Ashteyat, A., Obaidat, A., Kirgiz, M., et al. (2022). Production of roller compacted concrete made of recycled asphalt pavement aggregate and recycled concrete aggregate and silica fume. *International Journal of Pavement Research Technology, 15*, 987–1002. https://doi.org/10.1007/s42947-021-00068-4
34. Rakesh, P., Maddala, P., Priyanka, M. L., & Barhmaiah, B. (2021). Strength and behaviour of roller compacted concrete using crushed dust. *Materials Today: Proceedings*. https://doi.org/10.1016/j.matpr.2020.12.875
35. Tavakoli, D., Sakenian Dehkordi, R., Divandari, H., & de Brito, J. (2020). Properties of roller-compacted concrete pavement containing waste aggregates and nano SiO_2. *Construction and Building Materials, 249*, 118747. https://doi.org/10.1016/j.conbuildmat.2020
36. Lam, M.N.-T., Jaritngam, S., & Le, D.-H. (2017). Roller-compacted concrete pavement made of electric arc furnace slag aggregate: Mix design and mechanical properties. *Construction and Building Materials, 154*, 482–495. https://doi.org/10.1016/j.conbuildmat.2017.07
37. Madhkhan, M., Azizkhani, R., & Torki Harchegani, M. E. (2012). Effects of pozzolans together with steel and polypropylene fibers on mechanical properties of RCC pavements. *Construction and Building Materials, 26*(1), 102–112. https://doi.org/10.1016/j.conbuildmat.2011.05.009
38. Rahmani, E., Sharbatdar, M. K., & Beygi, H. A. M. (2020). A comprehensive investigation into the effect of water to cement ratios and cement contents on the physical and mechanical properties of roller compacted concrete pavement (RCCP). *Construction and Building Materials, 253*, 119177. https://doi.org/10.1016/j.conbuildmat.2020.11
39. Settari, C., Debieb, F., Hadj Kadri, E., & Boukendakdji, O. (2015). Assessing the effects of recycled asphalt pavement materials on the performance of roller compacted concrete. *Construction and Building Materials, 101*, 617–621.
40. Hesami, S., Modarres, A., Soltaninejad, M., & Madani, H. (2016). Mechanical properties of roller compacted concrete pavement containing coal waste and limestone powder as partial replacements of cement. *Construction and Building Materials, 111*, 625–635.
41. Bastani, M., & Behfarnia, K. (2020). Application of alkali-activated slag in roller compacted concrete. *Int. J. Pavement Res. Technol., 13*, 324–333. https://doi.org/10.1007/s42947-020-0088-y
42. Bayqra, S. H., Mardani-Aghabaglou, A., & Ramyar, K. (2022). Physical and mechanical properties of high volume fly ash roller compacted concrete pavement (a laboratory and case study). *Construction and Building Materials*. https://doi.org/10.1016/j.conbuildmat.2021.125664
43. Rooholamini, H., Sedghi, R., Ghobadipour, B., & Adresi, M. (2019). Effect of electric arc furnace steel slag on the mechanical and fracture properties of roller-compacted concrete. *Construction and Building Materials, 211*, 88–98. https://doi.org/10.1016/j.conbuildmat.2019.03.223
44. Rahmani, E., Sharbatdar, M. K., & Beygi, H. A. (2021). Influence of cement contents on the fracture parameters of Roller compacted concrete pavement (RCCP). *Construction and Building Materials, 289*, 123159. https://doi.org/10.1016/j.conbuildmat.2021.123159
45. Krishna, S., Rao, P., Sravana, T., & Rao, C. (2016). Experimental studies in Ultrasonic Pulse Velocity of roller compacted concrete pavement containing fly ash and M-sand. *International Journal of Pavement Research Technology, 9*, 289–301. https://doi.org/10.1016/j.ijprt.2016.08.003

46. Jahanbakhsh, P., Saberi, K. F., Soltaninejad, M., et al. (2022). Laboratory investigation of modified roller compacted concrete pavement (RCCP) containing macro synthetic fibers. *International Journal of Pavement Research Technology*. https://doi.org/10.1007/s42947-022-00161-2
47. Aghaeipour, A., & Madhkhan, M. (2017). Effect of ground granulated blast furnace slag (GGBFS) on RCCP durability. *Construction and Building Materials, 141*, 533–541. https://doi.org/10.1016/j.conbuildmat.2017.03.019
48. Aghayan, I., Khafajeh, R., & Shamsaei, M. (2020). Life cycle assessment, mechanical properties, and durability of roller compacted concrete pavement containing recycled waste materials. *International Journal of Pavement Research and Technology*. https://doi.org/10.1007/s42947-020-0217-7
49. Hazaree, C., Ceylan, H., & Wang, K. (2011). Influences of mixture composition on properties and freeze-thaw resistance of RCC. *Construction and Building Materials, 25*, 313–319.
50. Modarres, A., & Hosseini, Z. (2014). Mechanical properties of roller compacted concrete containing rice husk ash with original and recycled asphalt pavement material. *Materials & Design, 64*, 227–236. https://doi.org/10.1016/j.matdes.2014.07.072
51. Ghahari, S. A., Mohammadi, A., & Ramezanianpour, A. A. (2017). Performance assessment of natural pozzolan roller compacted concrete pavements. *Case Studies in Construction Materials, 7*, 82–90. https://doi.org/10.1016/j.cscm.2017.03.004
52. Algin, Z., & Gerginci, S. (2020). Freeze-thaw resistance and water permeability properties of roller compacted concrete produced with macro synthetic fibre. *Construction and Building Materials, 234*, 117382. https://doi.org/10.1016/j.conbuildmat.2019.11
53. Mardani-Aghabaglou, A., Andiç-Çakir, Ö., & Ramyar, K. (2013). Freeze–thaw resistance and transport properties of high-volume fly ash roller compacted concrete designed by maximum density method. *Cement and Concrete Composites, 37*, 259–266. https://doi.org/10.1016/j.cemconcomp.2013.01
54. Abbaszadeh, R., & Modarres, A. (2017). Freeze-thaw durability of non-air-entrained roller compacted concrete designed for pavement containing cement kiln dust. *Cold Regions Science and Technology, 141*, 16–27. https://doi.org/10.1016/j.coldregions.2017.05.007
55. Ashteyat, A. M., Al Rjoub, Y. S., Murad, Y., & Asaad, S. (2019). Mechanical and durability behaviour of roller-compacted concrete containing white cement by pass dust and polypropylene fibre. *European Journal of Environmental and Civil Engineering*. https://doi.org/10.1080/19648189.2019.1652694
56. Fakhri, M., & Saberik, F. (2016). The effect of waste rubber particles and silica fume on the mechanical properties of roller compacted concrete pavement. *Journal of Cleaner Production, 129*, 521–530. https://doi.org/10.1016/j.jclepro.2016.04.017
57. Boussetta, I., El, S., Khay, E., & Neji, J. (2018). Experimental testing and modelling of roller compacted concrete incorporating RAP waste as aggregates. *European Journal of Environmental and Civil Engineering, 8189*, 1–15. https://doi.org/10.1080/19648189.2018.1482792
58. Mardani-Aghabaglou, A., & Ramyar, K. (2013). Mechanical properties of high-volume fly ash roller compacted concrete designed by maximum density method. *Construction and Building Materials, 38*, 356–364. https://doi.org/10.1016/j.conbuildmat.2012.07.109
59. Debbarma, S., & Ransinchung, R. N. (2020). Achieving sustainability in roller compacted concrete pavement mixes using reclaimed asphalt pavement aggregates – state of the art review. *Journal of Cleaner Production*. https://doi.org/10.1016/j.jclepro.2020.125078
60. ASTM C128-15. (2015). *Standard test method for relative density (specific gravity) and absorption of fine aggregate*. ASTM International. www.astm.org.
61. ASTM C136/C136M-14. (2014). *Standard test method for sieve analysis of fine and coarse aggregates*. ASTM International. www.astm.org.
62. ASTM C1435/C1435M-14 (2014). *Standard practice for molding roller-compacted concrete in cylinder molds using a vibrating hammer*. ASTM International. www.astm.org
63. ASTM C138/C138M-17a. (2017). *Standard test method for density (unit weight), yield, and air content (gravimetric) of concrete*. ASTM International.
64. ASTM C642-13 (2013). Standard test method for density, absorption, and voids in hardened concrete. ASTM International. www.astm.org.
65. ASTM C39/C39M-18. (2018). *Standard test method for compressive strength of cylindrical concrete specimens*. ASTM International. www.astm.org.
66. ASTM C496/C496M-17. (2017). *Standard test method for splitting tensile strength of cylindrical concrete specimens*. ASTM International. www.astm.org.
67. ASTM C293/C293M-16. (2016) *Standard test method for flexural strength of concrete (using simple beam with center-point loading)*. ASTM International. www.astm.org.
68. ASTM C469/C469M-14. (2014). *Standard test method for static modulus of elasticity and poisson's ratio of concrete in compression*. ASTM International. www.astm.org.
69. ASTM C666/C666M-15. (2015). *Standard test method for resistance of concrete to rapid freezing and thawing*. ASTM International. www.astm.org.
70. ASTM C1723-16. *Standard guide for examination of hardened concrete using scanning electron microscopy*.
71. Berber, H., Tamm, K., Leinus, M.-L., Kuusik, R., Tõnsuaadu, K., Paaver, P., & Uibu, M. (2020). Accelerated carbonation technology granulation of industrial waste: effects of mixture composition on product properties. *Waste Management Research, 38*, 142–155. https://doi.org/10.1177/0734242X19886646
72. Radwan, M. M., Farag, L. M., Abo-El-Enein, S. A., & Abd El-Hamida, H. K. (2013). Alkali activation of blended cements containing oil shale ash". *Construction and Building Materials, 40*, 367–377.
73. ASTM C 1365-18. *Standard test method for determination of the proportion of phases in Portland cement and Portland-cement clinker using X-ray powder diffraction analysis*. ASTM International. www.astm.org.
74. Raado, L.-M., Kuusik, R., Hain, T., Uibu, M., & Somelar, P. (2014). Oil shale ash based stone formation hydration, hardening dynamics and phase transformations. *Oil Shale, 31*(1), 91–101. https://doi.org/10.3176/oil.2014.1.09
75. Omran, A., Harbec, D., Tagnit-Hamou, A., & Gagne, R. (2017). Production of roller-compacted concrete using glass powder: Field study. *Construction and Building Materials, 133*, 450–458. https://doi.org/10.1016/j.conbuildmat.2016.1
76. Portland Cement Association. (2010). *Guide for roller-compacted concrete pavements*.
77. Saad Issa Sarsam. (2020). Correlating the durability properties (porosity, density, and absorption) of roller compacted concrete pavement. *Journal of Cement Based Composites, 3*, 23–27.
78. Whitehurst, E. A. (1951). Soniscope test concrete structure. *J Am Concr Inst, 47*, 443–444.
79. Harrington, D., Abdo, F., Adaska, W., Hazaree, C. V., Ceylan, H., & Bektas, F. (2010). *Guide for roller-compacted concrete pavements*. In Trans Project Rep. 102.

Ahmed Ashteyat received a PhD in civil engineering from University of Akron, USA, in 2004 and MSc in structural engineering from Jordan University of Science and Technology in 2000. His research interests are fiber reinforced concrete, behavior of concrete under high temperatures, bond behavior of reinforcing steel and deteriorated concrete, durability aspects of fiber-reinforced concrete, nondestructive testing, self-compacting concrete and using of bi-products in concrete and pavement. He is currently a professor of civil engineering at University of Jordan.

Yousef Al Rjoub Ph.D University of Southern California, Civil Engineering May 2007. Currently is a professor in structural engineering at the Jordan University of Science and Technology. Research interest is Structural Analysis, Structural Dynamics, Earthquake Engineering, Finite Element Analysis, Finite Element Modeling Wave Propagation, Computational Mechanics, Finite Element Method.

Ala′ Obaidat received a PhD in civil Engineering from Concordia University, Canada, 2017 and MSc in structural engineering from Jordan University of Science and Technology in 2003. His research interests are fiber reinforced concrete, flexural and shear behavior of reinforced concrete beam, compression behaviour of reinforced concrete column, finite element analysis, masonry structure, column behavior of concrete under high temperatures, bond behavior of reinforcing steel and deteriorated concrete, durability aspects of fiber reinforced concrete, non-destructive testing, and self-compacting concrete. He is currently an assistant professor of Civil Engineering at Philadelphia University in Jordan.

Mehmet Kırgız is currently full professor at Istanbul Sabahattin Zaim University, Turkey. He began his professional working experience, including teaching in the graduate and undergraduate levels, research and development with TÜBİTAK and international institutions and universities collaboratively, and advising for students in their theses, in 1998. He also served as Vice dean, Member of Faculty Management Board, Member of Department Management Board in the aforementioned universities and institutions between 1998 years and 2021 years. He authored several peer-reviewed articles published in highly reputable outlets. Also, he has a national patent on cement manufacturing through the burning of marble powder and brick powder as farina. His major research and development interests are the broad fields of the binder and binder based materials, construction technology, infrastructure, sustainability, raw materials, mineralogy, upcycling, nanomaterials, and nanotechnology.

Mu′atsem Abdel-Jaber Professor of Structural Engineering. Ph.D. Civil Engineering/Structures university of Oxford Brookes UK. Currently is the Dean of Faculty of Engineering at Al-Ahliyya Amman University. His research interest: structural strengthening and repairing, durability aspects of fiber reinforced concrete, numerical modeling.

Amani Smadi obtained masters in Civil engineering/structure from Jordan University of Science and Technology in 2017. Her research interest is using of bi-product in concrete and pavement.